Inorganic Chemistry

Article

pubs.acs.org/IC

Homoleptic Gadolinium Amidinates as Precursors for MOCVD of Oriented Gadolinium Nitride (GdN) Thin Films

Michael Krasnopolski,[†] Cristian G. Hrib,[‡] Rüdiger W. Seidel,[§] Manuela Winter,[†] Hans-Werner Becker,[∥] Detlef Rogalla,[∥] Roland A. Fischer,[†] Frank T. Edelmann,*[,‡] and Anjana Devi*[,†]

[†]Lehrstuhl für Anorganische Chemie II, Ruhr-Universität Bochum, D-44801 Bochum, Germany

[‡]Lehrstuhl für Anorganische Chemie, Chemisches Institut, Otto-von-Guericke-Universität, Universitätsplatz 2, D-39106 Magdeburg, Germany

[§]Lehrstuhl für Analytische Chemie, Ruhr-Universität Bochum, D-44801 Bochum, Germany

[∥]Dynamitron-Tandem-Laboratorium (DTL) of RUBION, Ruhr-University Bochum, D-44801 Bochum, Germany

Supporting Information

ABSTRACT: Five new homoleptic gadolinium tris-amidinate complexes are reported, which were synthesized via the salt-elimination reaction of $GdCl_3$ with 3 equiv of lithiated symmetric and asymmetric amidinates at ambient temperature. The Gd-tris-amidinates $[Gd\{(N^iPr)_2CR\}_3]$ [R = Me (**1**), Et (**2**), ^{t}Bu (**3**), ^{n}Bu (**4**)] and $[Gd\{(NEt)(N^tBu)CMe\}_3]$ (**5**) are solids at room temperature and sublime at temperatures of about 125 °C (6×10^{-2} mbar) with the exception of compound **4**, which is a viscous liquid at room temperature. According to X-ray diffraction analysis of **3** and **5** as representative examples of the series, the complexes adopt a distorted octahedral structure in the solid state. Mass spectrometric (MS) data confirmed the monomeric structure in the gas phase, and high-resolution MS allowed the identification of characteristic fragments, such as $[\{(N^iPr)_2CR\}GdCH_3]^+$ and $[\{(N^iPr)_2CR\}GdNH]^+$. The alkyl substitution patterns of the amidinate ligands clearly show an influence on the thermal properties, and specifically, the introduction of the asymmetric carbodiimide leads to a lowering of the onset of volatilization and decomposition. Compound **5**, which is the first Gd complex with an asymmetric amidinate ligand system to be reported, was, therefore, tested for the MOCVD of GdN thin films. The as-deposited GdN films were capped with Cu in a subsequent MOCVD process to prevent postdeposition oxidation of the films. Cubic GdN on Si(100) substrates with a preferred orientation in the (200) direction were grown at 750 °C under an ammonia atmosphere and exhibited a columnar morphology and low levels of C or O impurities according to scanning electron microscopy, Rutherford backscattering, and nuclear reaction analysis.

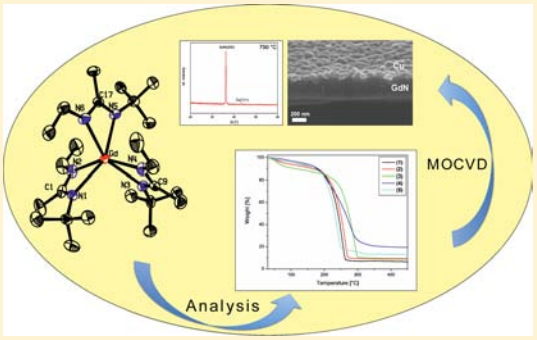

INTRODUCTION

Rare earth (RE) nitrides, such as gadolinium nitride (GdN) and dysprosium nitride (DyN), which are emerging materials for application in devices for spintronic applications, have been investigated from an experimental and theoretical point of view, only more recently.[1−7] RE nitride thin films, in general, have been less thoroughly studied in comparison to other metal nitrides not the least because of their strong oxophilic nature, which makes them very difficult to handle. Therefore, among the few reports available, sophisticated (high) vacuum physical vapor deposition (PVD) methods, such as molecular beam epitaxy (MBE),[8] ion-assisted deposition (IAD),[9] or Ar/N_2 mixed-gas-plasma radio frequency (rf) sputtering, were necessary to deposit these layers.[10] However, metal-organic chemical vapor deposition (MOCVD) is a technique of choice for device mass production in view of the advantages, such as large area deposition, good composition control, film uniformity, and good conformal coverage on nonplanar geometries. Nevertheless, there are hardly any reports on MOCVD-grown RE nitrides because of a dearth of suitable rare earth precursors, which are volatile as well as contain ligands that are free of oxygen. Most of the RE precursors reported contain an oxygen coordination sphere, which are unsuitable for RE nitrides. We were the first to report on the deposition of GdN and DyN MOCVD using the guanidinate and amidinate class of precursors.[11,12] Apart from these studies, there is only one additional report on the deposition of RE nitride thin films by CVD in which an RE halide ($GdCl_3$) was used together with ammonia as a reactive gas at temperatures as high as 900 °C.[13] In general, an MOCVD precursor should possess sufficient volatility, good thermal stability, and a clean decomposition pathway. RE precursor chemistry has been discussed recently by Edelmann et al.[14] One class of oxygen-free RE complexes are the monomeric and volatile RE bis(trimethylsilyl)amides. They were only used for ALD of RE oxides, but they had the drawback of silicon

Received: August 21, 2012
Published: December 11, 2012

   dx.doi.org/10.1021/ic301826s | *Inorg. Chem.* 2013, 52, 286−296

Scheme 1. Synthesis of the Homoleptic Rare Earth Amidinates

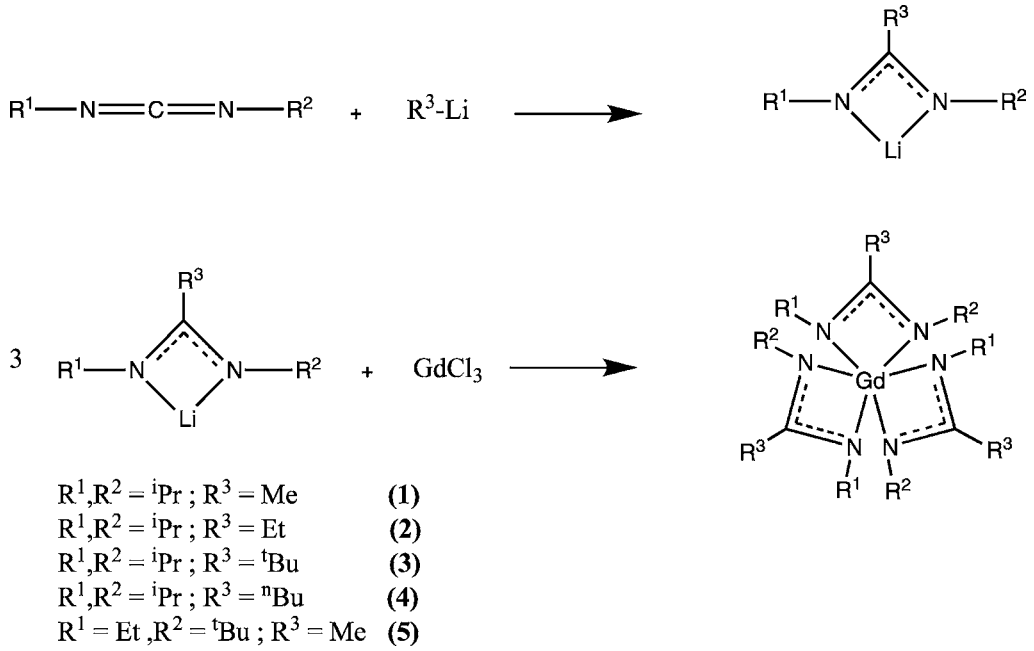

$R^1,R^2 = {}^{i}Pr\,;\ R^3 = Me$ **(1)**
$R^1,R^2 = {}^{i}Pr\,;\ R^3 = Et$ **(2)**
$R^1,R^2 = {}^{i}Pr\,;\ R^3 = {}^{t}Bu$ **(3)**
$R^1,R^2 = {}^{i}Pr\,;\ R^3 = {}^{n}Bu$ **(4)**
$R^1 = Et\ ,R^2 = {}^{t}Bu\,;\ R^3 = Me$ **(5)**

incorporation in the deposited films.[15−20] However, the ammonolysis of these compounds yielded bulk rare earth nitrides via a sol−gel-like chemistry.[21,22] Another type of rare earth precursor are the tris-cyclopentadienyls (Cps). The complexes are thermally stable and show suitable volatility, which is dependent on the metal center and on the modification of the Cp-ligands.[23] These compounds were mainly used for ALD of various RE oxides,[24−28] and in terms of MOCVD, they were used as precursors for RE doping of GaAs or InP semiconductors.[29,30] These compounds also have been used in ammonolysis reactions to yield bulk rare earth nitrides.[31] Nevertheless, the use of homoleptic cyclopentadienyl complexes of RE as precursors for RE nitride MOCVD in the presence of ammonia may cause heavy C-incorporation. All-nitrogen coordinated RE amidinates and guanidinates are promising classes of precursors for RE-containing materials, which hold promise to overcome these problems and have been demonstrated to be suitable for ALD of RE oxides and as well as MOCVD of RE nitrides.[32−37] While the RE guanidinates favored the formation of RE nitrides, allowing even a single source precursor (SSP) approach, the RE amidinates needed an additional source of nitrogen (NH_3) for the deposition of impurity-free RE nitrides.[12]

In our pursuit of new or alternative RE precursors with improved thermal properties, we have explored the RE amidinate chemistry further, and herein, we report the synthesis and characterization of five new homoleptic gadolinium tris-amidinate complexes $[Gd\{(N^{i}Pr)_2CR\}_3]$ [R = Me (**1**), Et (**2**), ^{t}Bu (**3**), ^{n}Bu (**4**)], and $[Gd\{(NEt)(N^{t}Bu)CMe\}_3]$ (**5**). Single-crystal structural analysis performed on compounds **3** and **5** revealed that they are monomers. The thermal properties were examined in view of their potential application as precursors, and mass spectrometric analysis was employed to gain an insight into the possible decomposition pathways of the complexes. As a proof of principle, the most volatile precursor with the asymmetric amidinate ligand, compound **5**, was chosen in combination with NH_3 for the deposition of GdN thin films on Si(100) substrates. Preliminary analytical investigation on the obtained layers was performed, employing X-ray diffraction, scanning electron microscopy (SEM), and a combination of Rutherford backscattering and nuclear reaction analysis, and the salient features of the data obtained are highlighted.

RESULTS AND DISCUSSION

Synthesis and Characterization. The syntheses of the homoleptic RE amidinates are carried out following a modified route published by Dröse et al.[38] At first, the lithiated *N,N′*-dialkyl-amidinato ligands $[Li\{(NR^1)(NR^2)CR^3\}]$ are prepared by the reaction of *N,N′*-diisopropyl-carbodiimide with four different lithium alkyls, LiR (R = Me, Et, ^{t}Bu, ^{n}Bu), and *N,N′*-^{t}butyl-ethyl-carbodiimide with LiMe in THF, following the general synthetic route for the synthesis of lithium guanidinates published by Aeilts et al.[39] Because the reaction gives a nearly quantitative yield of the lithiated amidinato ligand, the freshly prepared solutions of the corresponding lithium amidinates $[Li\{(N^{i}Pr_2)CR\}]$ [R = Me (**1**), Et (**2**), ^{t}Bu (**3**), ^{n}Bu (**4**)] and $[Li\{(NEt)(N^{t}Bu)CMe\}]$ (**5**) are used in the subsequent salt metathesis reactions without further purification. Afterward, a slurry of $GdCl_3$ in THF with 3 equiv of the corresponding lithium amidinate affords the series of homoleptic tris-*N,N′*-dialkyl-2-alkyl-amidinato gadolinium complexes $[Gd\{(NR^1)(NR^2)CR^3\}_3]$ displayed in Scheme 1.

The reactions are completed within 12 h, and after workup, the gadolinium amidinates **1**−**5** are isolated in reasonable yields (50−80%) as white to pale yellow crystalline solids. The products are soluble in common organic solvents, such as THF, Et_2O, pentane, or hexane, and are purified by recrystallization, followed by sublimation as outlined in the Experimental Section in detail. Upon recrystallization, single crystals are obtained, but in most cases, the quality of the crystals was poor. However, we obtained crystals of compounds **3**·0.5 C_5H_{12} and **5** suitable for single-crystal X-ray diffraction, and the molecular structures in the solid state were determined.

Crystals of **3**·0.5 C_5H_{12} and **5** were obtained by recrystallization from *n*-pentane. The X-ray analyses reveal the anticipated mononuclear homoleptic gadolinium(III) complexes, in which the Gd^{3+} metal center is coordinated by three chelating amidinato ligands (Figure 1). The crystal structure of **3**·0.5

dx.doi.org/10.1021/ic301826s | Inorg. Chem. 2013, 52, 286−296

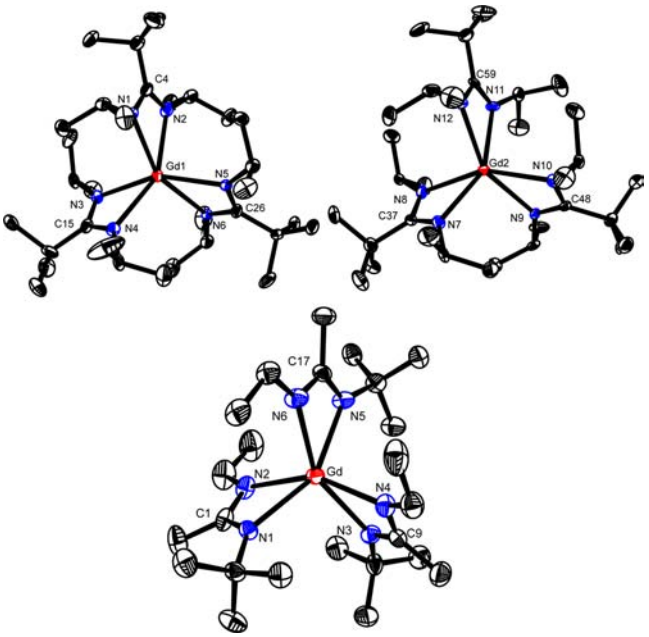

Figure 1. Molecular structures of $[Gd\{(N^iPr)_2C^tBu\}_3]$ (**3**) (top; molecule 1 left, molecule 2 right) and $[Gd\{(NEt)(N^tBu)CMe\}_3]$ (**5**) (bottom) in the solid state. Hydrogen atoms omitted for clarity. The thermal ellipsoids are drawn at 50% probability (Gd = red, N = blue, C = black).

C_5H_{12} contains two crystallographically distinct molecules of **3**, one of which shows rotational disorder of a *tert*-butyl group. Compound **5** shows helical chirality. It crystallizes in the centrosymmetric monoclinic space group $P2_1/n$ with four molecules in the unit cell. These molecules occur due to the space group symmetry (see Table 1). In the unit cell, there are two

Table 1. Crystallographic Data of 3·0.5 C_5H_{12} and 5

	3·0.5 C_5H_{12}	5
empirical formula	$C_{33}H_{69}N_6Gd·0.5\ C_5H_{12}$	$C_{24}H_{51}N_6Gd$
M_r	743.27	580.96
T (K)	106(2)	143(2)
λ (Å)	0.71073	0.71073
cryst size (mm^3)	0.29 × 0.28 × 0.26	0.30 × 0.07 × 0.05
cryst syst	triclinic	monoclinic
space group	$P\bar{1}$	$P2_1/n$
a (Å)	11.4022(5)	9.5303(19)
b (Å)	19.3686(11)	19.620(4)
c (Å)	21.2344(16)	15.667(3)
α (deg)	115.814(7)	90
β (deg)	92.061(4)	99.80(3)
γ (deg)	107.022(4)	90
V ($Å^3$)	3963.2(4)	2886.6(10)
Z	4	4
data/restraints/params	19257/87/759	5868/0/280
$2\theta_{max}$ (deg)	50	52
GOF on F^2	0.945	1.010
R_1 [$I > 2\sigma(I)$]	0.0405	0.0592
wR_2 (all data)	0.0935	0.0939
residuals (e $Å^{-3}$)	1.291/−1.543	0.903/−1.778

Λ- and two Δ-stereoisomers. The fact that a Δ-stereoisomer forms the asymmetric unit is a coincidence because the synthesis was not enantiopure. In both compounds **3** and **5**, the coordination sphere of Gd^{3+} is best described as a severly distorted octahedron. The distortion from the regular octahedral shape is attributed to the bite angle of the amidinato ligands. Selected bond lengths and angles are listed in Table 2. The Gd−N bond lengths and N−Gd−N bond angles are within expected ranges and are in good agreement to the values known in the literature.[34,35,38] The Gd−N bond lengths range from 2.385(5) to 2.414(7) Å (average 2.401 Å) for compound **3** and from 2.385 to 2.419 Å (average 2.402 Å) for compound **5**. Compared to the closely related gadolinium guanidinate $[Gd\{(N^iPr)_2CNMe_2\}_3]$, the bond lengths are slightly increased (2.384 Å).[40] As expected, the GdNCN chelate rings are essentially planar. The ligands show bite angles of 110.7−112.4° (NCN) and 54.60−55.18° (NGdN), which is also in good agreement with the literature.[34,35,38] The features of the molecular structures of the other compounds is expected to be similar based on the similar compositions with small variations of R^1 and R^2 and the results obtained from mass spectroscopy that are presented later on.

Mass Spectrometry. The influence of ligand variation on the fragmentation behavior of the complexes was investigated, employing mass spectrometric analysis. Although the decomposition mechanism in a CVD process cannot be directly compared to the fragmentation mechanism under mass spectrometric conditions, this characterization is certainly useful to see the stability of the compounds under gas-phase ionization conditions. Moreover, since the CDI deinsertion is a possible route in amidinate-based complexes,[41] we were keen to see whether such a phenomenon takes place in the Gd compounds as this cannot be easily proved from NMR measurements due to the strong paramagnetic nature of the Gd^{3+} ion. Therefore, EI-MS was performed on all the complexes, and as seen from Figure 2 and Figure SI 1 (Supporting Information), similar patterns of fragments are observed for all the compounds, indicating that these complexes decompose in a similar pathway under mass spectrometric conditions. Complexes **1**, **2**, and **5** are discussed in some detail, and a possible decomposition mechanism is deduced from the data obtained. The origin of all visible mass envelopes can be nicely explained, and the assigned fragments of **1**−**5** are summarized in Table 3.

In all fragmentation patterns, the molecular ion peak (M+) with a relative intensity of 21% (**1**), 10% (**2**), 3% (**3**), 9% (**4**), and 3% (**5**) is detected. The peaks of the molecular ions are confirmed by high-resolution mass spectroscopy (HR-MS). No peaks with higher m/z are detected so that the suggested monomeric structure of **1**−**5** in the gas phase is confirmed. The first fragmentation steps can be assigned to the cleavage of a methyl group ($M^+ - 15$) and an isopropyl group ($M^+ - 43$) from one of the amidinato ligands. After the subsequent loss of the rest of one ligand, the ML_2^+ fragments for **1** (m/z = 440), **2** (m/z = 466), **3** (m/z = 526), **4** (m/z = 524), and **5** (m/z = 440) can be clearly identified. All further peaks are assigned to distinctive fragmentation products of the molecular ions of **1**−**5**.

Special attention is given to the mass peaks at m/z = 314 (**1**), m/z = 328 (**2**), m/z = 353 (**3**), m/z = 357 (**4**), and m/z = 314 (**5**), respectively. From the mass spectrometry data, a distinction between two likely fragments is not possible. One such species consists of a gadolinium center coordinated by one amidinato ligand and a methyl group, for example, $[\{(N^iPr)_2CR\}GdCH_3]$ and another species containing a gadolinium center coordinated by one amidinato ligand and one imido group, for example, $[\{(N^iPr_2)_2CR\}GdNH]$. For compounds **1** and **5**, the HR EI-MS data reveal that the mass envelope belongs to the Gd-alkyl species, where a methyl group is bound to the metal center as we also found earlier for related compounds.[11] This assignment

dx.doi.org/10.1021/ic301826s | Inorg. Chem. 2013, 52, 286−296

Table 2. Averages of Selected Bond Lengths [Å] and Angles [deg] of 3, 5, and Reference Compound

	$[(N^iPr)_2{}^tBuC]_3Gd$ molecule 1 (3)	$[(N^iPr)_2{}^tBuC]_3Gd$ molecule 2 (3)	$[(N^tBu)(NEt)MeC]_3Gd$ (5)	$[(N^iPr)_2CNMe_2]_3Gd$[40]
Gd−N (bond length)	2.401	2.402	2.402	2.410
N−C (bond length)	1.338	1.338	1.333	1.335
N−Gd−N (angle)	54.9	54.9	55.6	55.9
N−C−N (angle)	111.6	111.7	114.3	115.4

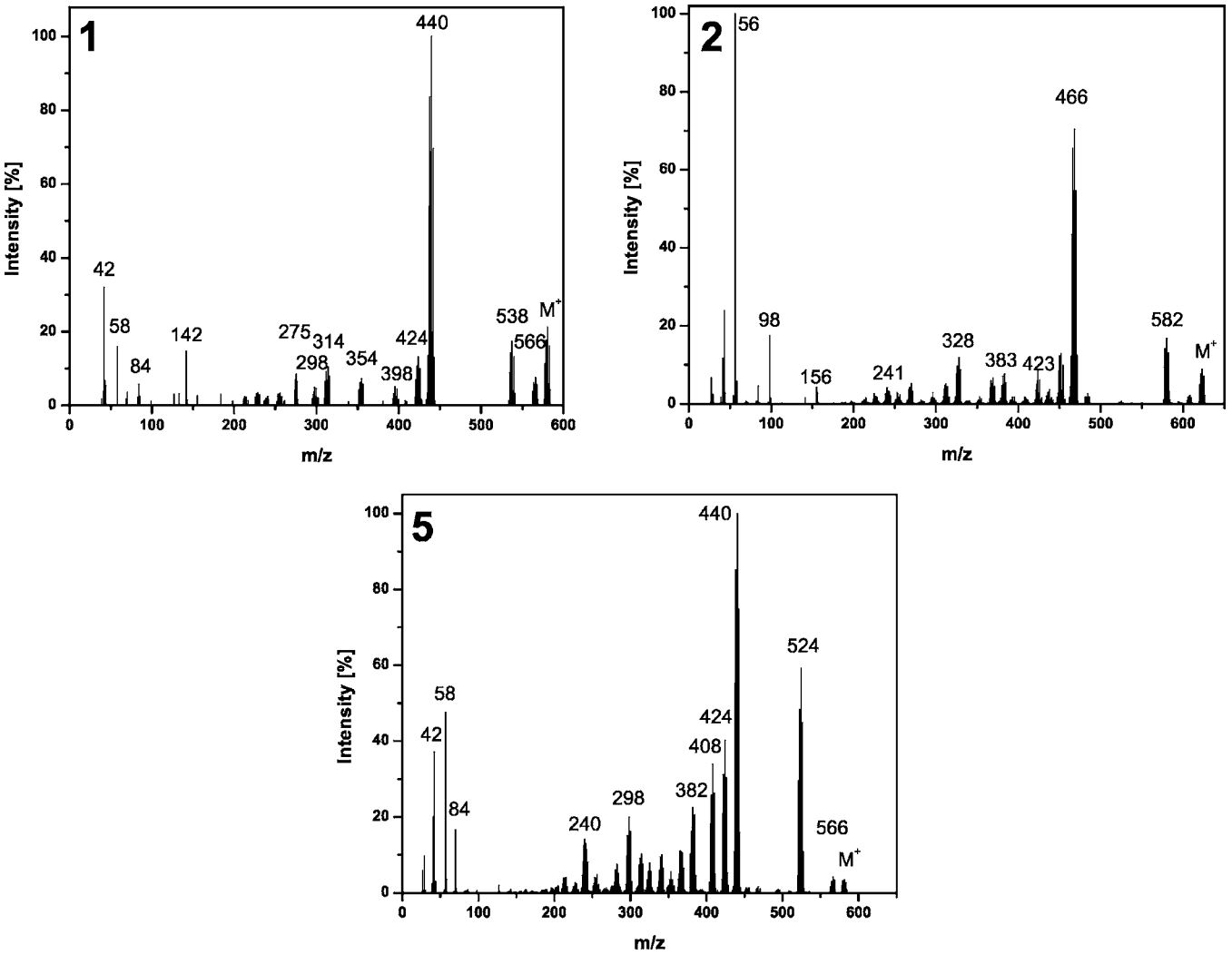

Figure 2. EI-MS spectra of compounds 1 (top left), 2 (top right), and 5 (bottom).

is further substantiated by the insignificant deviation of the observed mass from the calculated mass of this fragment. Similar results are observed for compounds 1, 4, and 5. However, HR EI-MS data of compounds 2 and 3 show different results. For these compounds, a Gd-imido species is observed and confirmed, which is analogous to the RE-guanidinates $[Gd\{(N^iPr)_2CNMe_2\}_3]$ reported by Milanov et al.[12] This comparison suggests a different behavior of the modified amidinates under MOCVD conditions. It is possible that compounds 2 and 3 are more suitable as single source precursors (SSPs) for the rare earth nitrides (RENs) than compound 1 (which has been proven not to be a useful SSP for REN thin films).[11] One possible reason for this different behavior is that, for compounds 2 and 3, a β-H-elimination (Scheme 2) of the terminal alkyl group can occur, whereas for compounds 1, 4, and 5, such an elimination process seems not to be favorable. Additionally, it should be noted that, for compounds 1, 2, and 5, no peaks for *N,N′*-dialkylcarbodiimide are observed, which indicates that no carbodiimide deinsertion reaction takes place and that the compound can be transported in the gas phase without a predecomposition. For compounds 3 and 4, these CDI-peaks are observed with intensities below 10%.

Selected fragments are presented in Figures 3 and 4. Although the presented EI-MS spectra indicate a defined and clean decomposition of the complexes without any hint of a carbodiimide deinsertion, it should be noted with caution that these results are obtained under mass spectrometric conditions, where ionic species are involved. To investigate the decomposition behavior of the rare earth amidinates (1−5) under CVD conditions, additional decomposition analysis, such as, for example, matrix isolation or TG-MS analyses, are necessary, but this is beyond the scope of this work.

Thermal Properties. The primary goal of synthesizing a homologous series of tris-amidinato gadolinium compounds was, on the one hand, driven by our interest to see the effect of

dx.doi.org/10.1021/ic301826s | Inorg. Chem. 2013, 52, 286−296

Table 3. Overview of the Selected Fragments of Complexes 1–5 Observed in Mass Spectra

compd 1 fragments[a]	mass	$[m/z]^a$ int. [%][a]	compd 2 fragments[a]	mass	$[m/z]^a$ int. [%][a]	compd 3 fragments[a]	mass	$[m/z]^a$ int. [%][a]	compd 4 fragments[a]	mass	$[m/z]^a$ int. [%][a]	compd 5 fragments[a]	mass	$[m/z]^a$ int. [%][a]
$M^+/[GdL_3]^+$	581	21	$M^+/[GdL_3]^+$	623	9	$M^+/[GdL_3]^+$	707	2	$M^+/[GdL_3]^+$	707	9	$M^+/[GdL_3]^+$	581	3
$M - CH_3^+$	566	8	$M - CH_3^+$	n.d.		$M - CH_3^+$	n.d.		$M - CH_3^+$	n.d.		$M - CH_3^+$	566	4
$M - {}^iPr^+$	538	17	$M - {}^iPr^+$	580	17	$M - {}^iPr^+$	n.d.		$M - {}^iPr^+$	666	25	$M - {}^tBu^+$	524	59
$[(L_2)Gd]^+$	440	100	$[(L_2)Gd]^+$	468	70	$[(L_2)Gd]^+$	526	100	$[(L_2)Gd]^+$	524	100	$[(L_2)Gd]^+$	440	100
$[(L_2)Gd(-CH_3)]^+$	424	13	$[(L_2)Gd(-CH_3)]^+$	452	12	$[(L_2)Gd(-CH_3)]^+$	508	8	$[(L_2)Gd(-CH_3)]^+$	509	19	$[(L_2)Gd(-CH_3)]^+$	424	40
$[(L)Gd\{N_2CR\}]^+$	355	7	$[(L)Gd\{N_2CR\}]^+$	383	8	$[(L)Gd\{N_2CR\}]^+$	439	9	$[(L)Gd\{N_2CR\}]^+$	440	13	$[(L)Gd\{N_2CR\}]^+$	354	6
$[(CH_3)Gd(L)]^+$	314	11	$[(NH)Gd(L)]^+$	328	12	$[(NH)Gd(L)]^+$	356	12	$[(CH_3)Gd(L)]^+$	357	15	$[(CH_3)Gd(L)]^+$	314	6
$[Gd(L)]^+$	298	5	$[Gd(L)]^+$	n.d.		$[Gd(L)]^+$	340	6	$[Gd(L)]^+$	340	8	$[Gd(L)]^+$	298	20
L^+	142	15	L^+	155	4	L^+	184	8	L^+	185	6	L^+	n.d.	
$[CDI]^+$	n.d.		$[CDI]^+$	n.d.		$[CDI]^+$	127	11	$[CDI]^+$	127	6	$[CDI]^+$	127	2
$[\{N^iPr\}NC]^+$	84	6	$[\{N^iPr\}NC]^+$	n.d.		$[\{N^iPr\}NC]^+$	84	88	$[\{N^iPr\}NC]^+$	83	8	$[CDI]^+ - 3CH_3$	84	17
$[HN^iPr]^+$	58	16	$[HN^iPr]^+$	56	100	$[HN^iPr]^+$	57	45	$[HN^iPr]^+$	57	42	$[MeNEt]^+$	58	48
$[^iPr]^+$	42	32	$[^iPr]^+$	43	24	$[^iPr]^+$	42	29	$[^iPr]^+$	42	30	$[NEt]^+$	42	37

[a]n.d. = not detected, L = complete ligand, CDI = respective dialkylcarbodiimide.

Scheme 2. β-H-Elimination

ligand variation on the thermal properties and decomposition characteristics and, on the other hand, by tuning the volatility of the Gd complexes with respect to their use as precursors for MOCVD of Gd-containing thin films. In this context, thermogravimetric analysis (TGA) and isothermal TG studies were employed to investigate the volatility and thermal stability of **1**–**5**.

As seen in TGA plots (Figure 5), compounds **1**–**5** exhibit a similar volatilization behavior in a single step. However, the onset temperature of volatilization varies, and this shows that the structure of the ligand surrounding the Gd metal center influences the volatility of the complexes. In the case of compound **3**, the step observed at low temperatures can be attributed to a solvent molecule (pentane) that is visible in the crystal structure. The initial step in all the cases at 25 °C is due to the partial decomposition of the precursor upon a short exposure to ambient air when loading the precursor for TG measurements.

For compounds **1**, **2**, and **4**, the onset temperatures of vaporization (ca. 210 °C) are quite similar, but there is a change in the decomposition temperature where the weight loss ceases and a constant rest mass is left beyond a certain temperature. For example, the decomposition temperature is about 260 °C (**1**), 270 °C (**2**), and 310 °C (**4**). The temperature onset of volatilization is shifted to higher temperatures in the case of compound **3** (220 °C), and the decomposition temperature is also accordingly shifted (310 °C). In the case of compound **5**, the precursor volatilizes at a much lower temperature (around 170 °C) and decomposes at 250 °C. This clearly indicates that the lower molecular mass as well as the asymmetry in the ligand sphere is beneficial for raising the volatility of the complex.

Comparing these data with those reported for $[Y\{(N^iPr)_2CMe\}_3]$ (onset = ca. 225 °C, decomposition = 285 °C)[32] and for $[Gd\{(N^iPr)_2CNMe_2\}_3]$ (onset = ca. 220 °C, evaporation end = ca. 267 °C),[40] it is obvious that there is a close similarity in the thermal behavior of the guanidinato and amidinato complexes, although the molecular mass of the amidinato complex is about 15% lower than that of the corresponding guanidinato complex bearing the same rare earth center. This also shows very clearly that not only the molecular masses of the compounds but also intermolecular interactions in the crystalline or liquid phase have a strong influence on their thermal behavior.

dx.doi.org/10.1021/ic301826s | Inorg. Chem. 2013, 52, 286–296

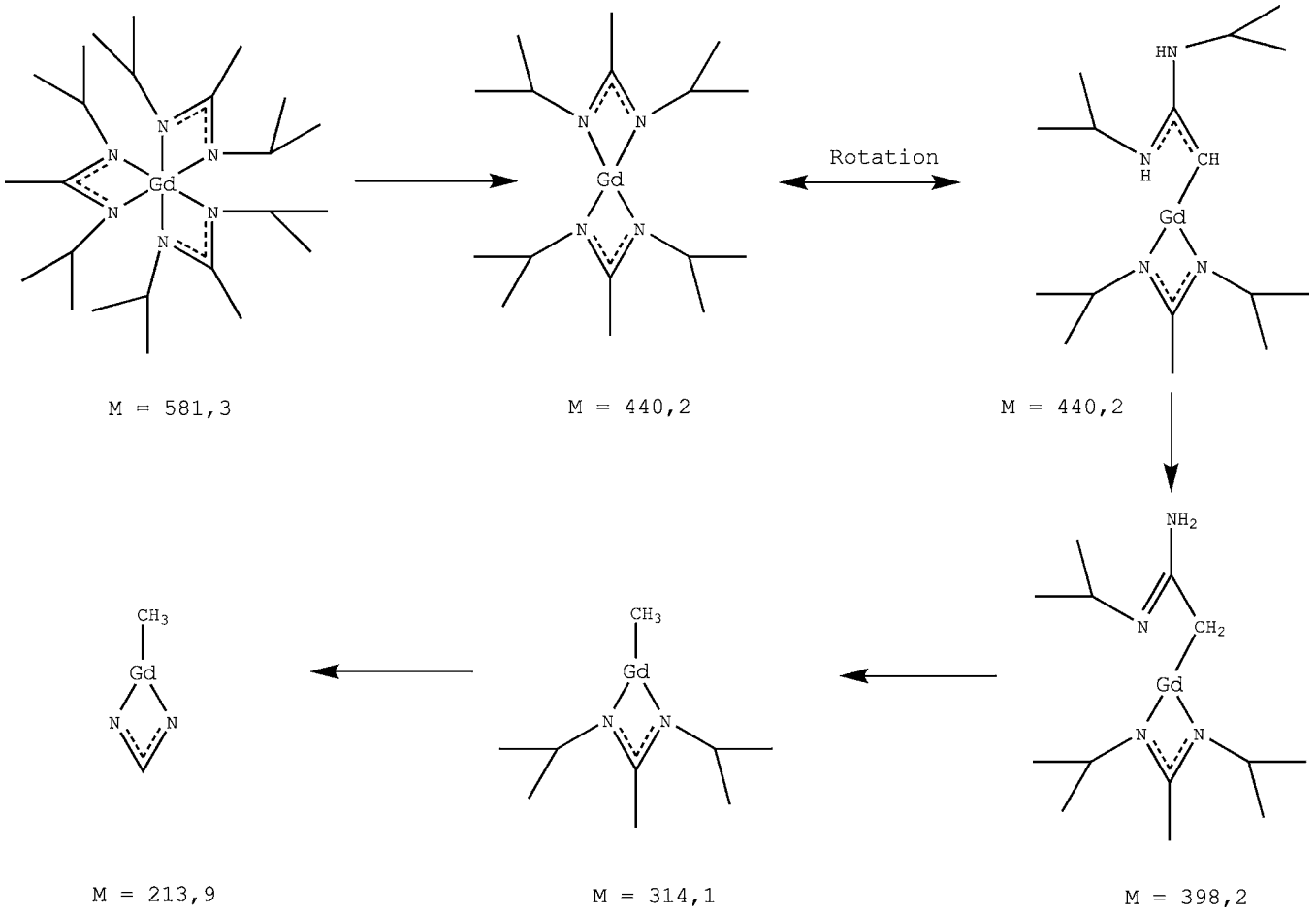

Figure 3. Selected fragments observed in the EI-MS spectrum of compound **1**. Compound **5** shows a similar fragmentation with matching masses.

The residual masses, left behind after precursor decomposition, are of the order of 9% (**1**), 10% (**2**), 11% (**3**), 21% (**4**), and 15% (**5**). The expected theoretical mass for the formation of GdN, assuming that the precursor decomposes cleanly, is 24−30%. However, the values are much less than the expected masses, and this indicates that there is a volatilization process coupled with partial decomposition at higher temperatures. These masses can also be partially attributed to the fact that the TGA instrument is operated under ambient conditions outside a glovebox using an inert gas flow (N_2) during the measurement. For these air-sensitive rare earth compounds, this can lead to a partial hydrolysis/oxidation and thus to higher residual masses.

The thermal behavior of **1**−**5** was further investigated by isothermal TGA analysis. Figure 6 shows isothermal TGA of the most volatile amidinate presented here, namely, compound **5**, at two different temperatures of 100 and 120 °C. At each fixed temperature, the mass loss is measured for a long period of time (400 min). In the measurements of all compounds, an almost linear weight loss is observed, which indicates that, at these conditions, only sublimation takes place and no decomposition has to be taken into account. From the slopes of the corresponding curves, the evaporation rates at different temperatures are determined. The evaporation rates at 100−120 °C are in the range of 8−41 μg min^{-1} cm^{-2}. Table 4 summarizes some physical properties of **1**−**5**.

From the thermal studies, we conclude that, among the rare earth amidinates reported here, the complexes **1**, **2**, and **5** show promising properties for MOCVD. The use of **1** in MOCVD experiments was reported earlier.[11] Because compound **5** shows improved thermal properties with highest sublimation rates and a broad temperature window between sublimation and decomposition, it was chosen for the application in MOCVD of GdN films.

Precursor Evaluation for MOCVD of GdN Thin Films. In the first set of experiments, compound **5** was employed for the deposition without any additional nitrogen source and examined if this route results in the formation of GdN following a single source precursor (SSP) approach. Indeed, thin films are obtained on Si(100) substrates with growth rates of the order of 5−50 nm/min in the temperature range of 450−850 °C (SI 2, Supporting Information). When examined by XRD, the films are amorphous even when the temperatures are as high as 850 °C (Figure 7). The only reflexes visible in the XRD pattern are due to the Si substrate and the Cu film (capping layer). From the RBS analysis presented in the following section, it is found that the films constitute mainly GdCN.

In the second case, ammonia is used as an additional source of nitrogen and all other CVD process parameters are maintained the same. This route yields GdN thin films in the temperature range of 450−850 °C with growth rates in the order of 20−35 nm/min (see SI 2, Supporting Information). The onset of crystallization of GdN films of the rock salt structure is 650 °C. The reflexes at 2θ values of 32, 36, and 52° are indexed as the (111), (200), and (220) reflexes of fcc-GdN, respectively. As the substrate temperature is increased to 750 °C,

dx.doi.org/10.1021/ic301826s | *Inorg. Chem.* 2013, 52, 286−296

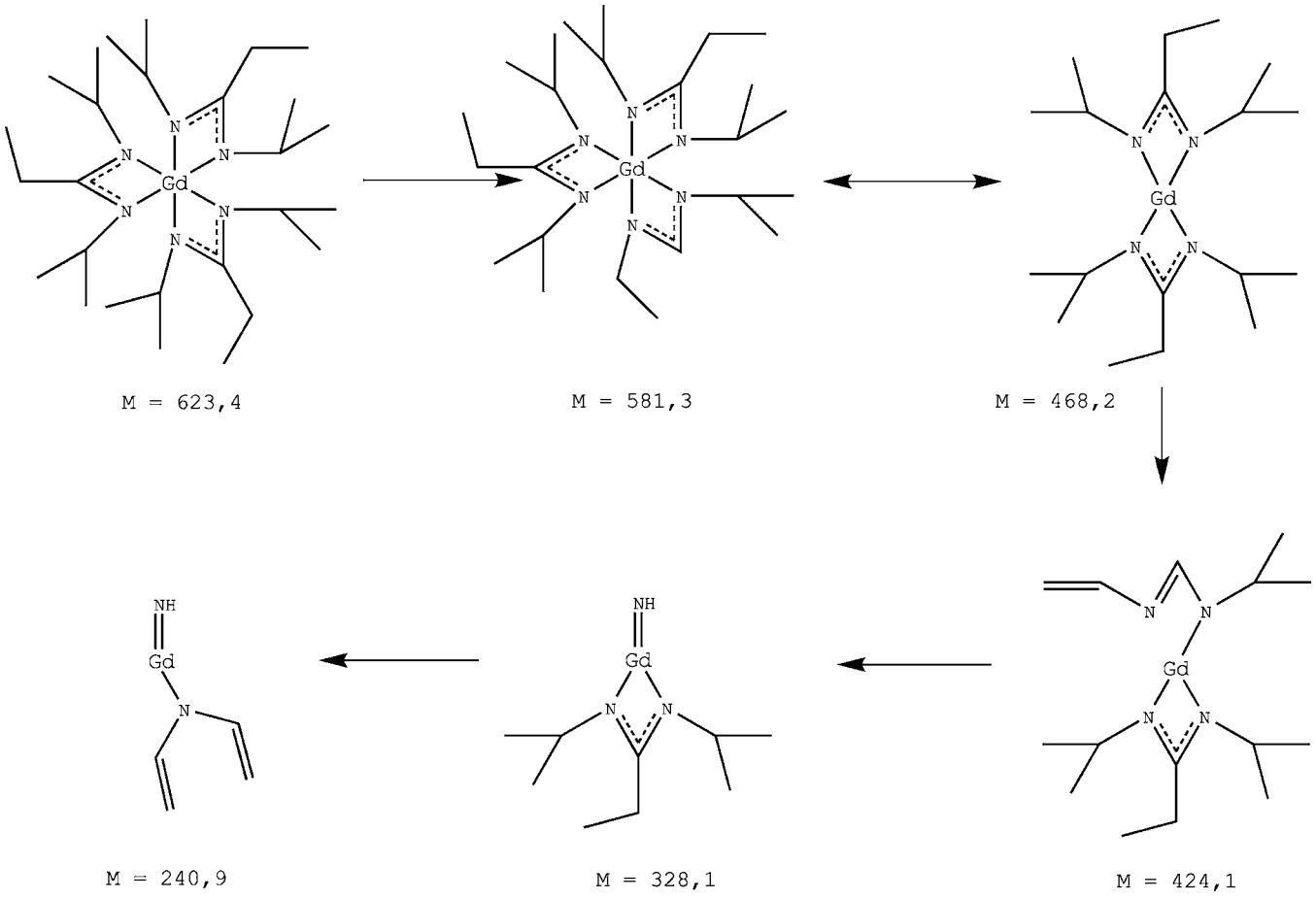

Figure 4. Selected fragments observed in the EI-MS spectrum of compound **2**.

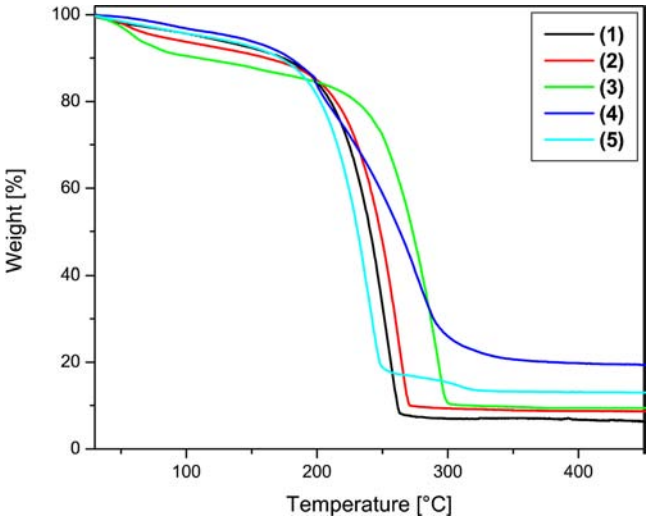

Figure 5. TGA plots of $[Gd\{(NR^1)(NR^2)CR^3\}_3]$ (**1**–**5**).

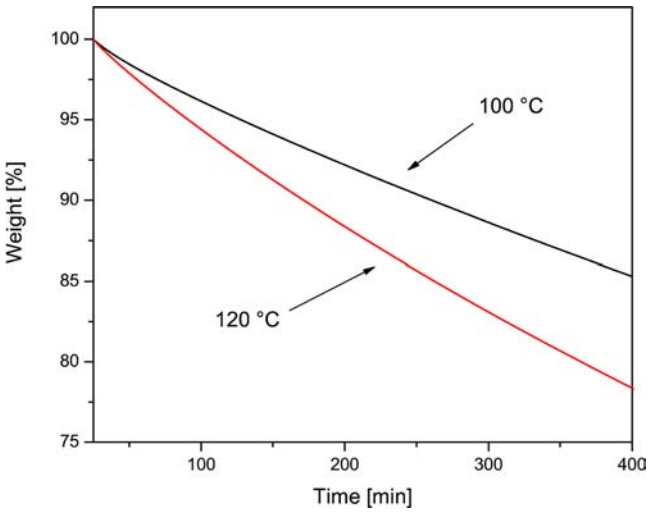

Figure 6. Isothermal TG analysis of compound **5** at 100 and 120 °C for 400 min.

we obtain GdN in the cubic phase with a preferred orientation in the (200) direction (Figure 8). The Cu capping leads to a reflex at $2\theta = 43°$ in the (111) orientation.

The morphology of the as-deposited films was further investigated with SEM, and as seen in Figure 9, the films grown under SSP conditions consist of a nearly amorphous matrix of about 50–550 nm in thickness capped with the Cu layer (60 nm). When ammonia is used, the films seem to be polycrystalline, evidenced by the presence of some longitudinal grains with a columnar-type structure. An uneven, but clear, interface between the Cu and the GdN layer is observed, and the Cu layer appears to be rough and consists of densely packed grains on the top of the GdN layer.

To determine the average coherence length of the crystalline domains in the films deposited at 750 and 850 °C using compound **5**, the full width at half-maximum (fwhm) of the corresponding (200) peak is determined and subsequently applied to

dx.doi.org/10.1021/ic301826s | *Inorg. Chem.* 2013, 52, 286–296

Table 4. Thermal Properties of Gadolinium Amidinato Complexes 1−5

	onset of vaporization [°C]	residual mass after TGA [%]
1	208	9
2	208	10
3	250	11
4	210	21
5	195	15

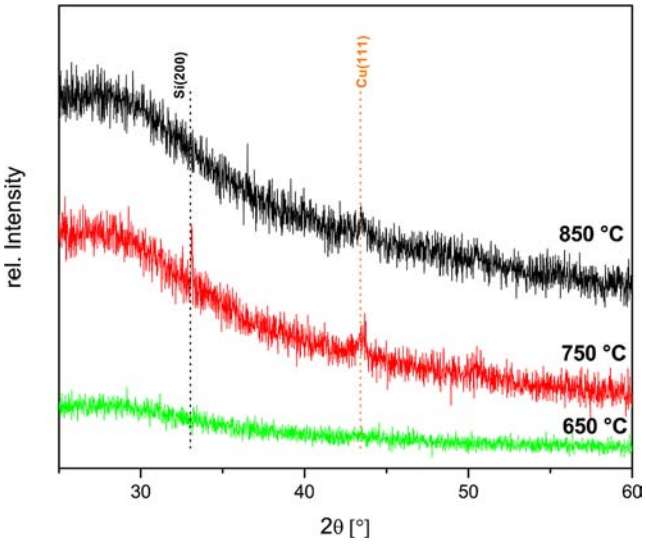

Figure 7. X-ray diffraction patterns of GdN grown on Si(100) at 650−850 °C using **5** as precursor in SSP conditions (peaks indexed according to JCPDS no. 00-015-0888).

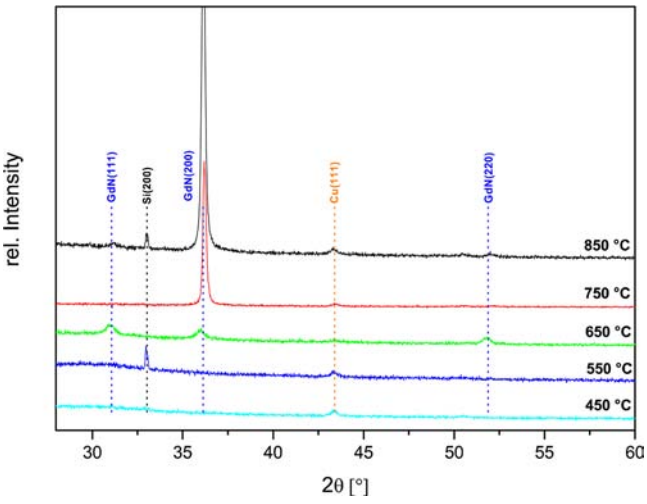

Figure 8. X-ray diffraction patterns of GdN grown on Si(100) at 450−850 °C using **5** as precursor in the presence of ammonia (peaks indexed according to JCPDS no. 00-015-0888).

the Scherrer equation.[42] The average crystallite size is estimated to 35−40 nm. It is reported that impurities cause significant changes in the lattice constant of fcc-RE nitrides,[43] so the lattice constants of the GdN films are calculated from the position of the predominant (200) reflections to evaluate the quality of the films. The results are listed in Table 5. The obtained lattice parameter values of the deposited GdN films range from 4.971 ± 0.005 to 4.977 ± 0.005 Å, which fits well with the lattice

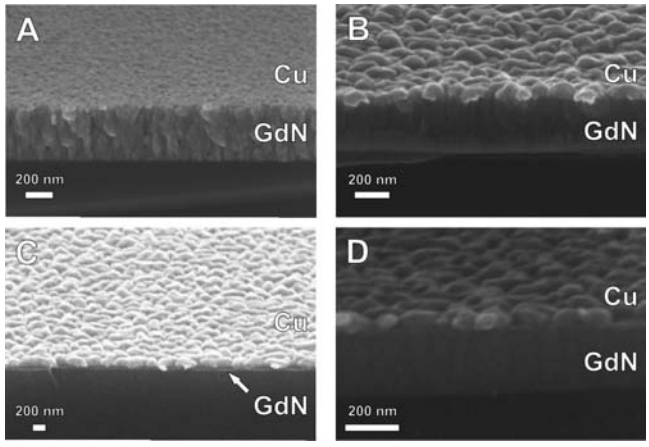

Figure 9. Representative SEM images of films deposited at 750 and 450 °C as SSP (A and C) and with ammonia as reactive gas (B and D).

parameter values of unstrained fcc-GdN (4.999 ± 0.005 Å; The International Center for Diffraction Data PDF (Powder Diffraction file) JCPDS no. 00-015-0888) The lattice parameter values of the deposited GdN thin films are comparable to the lattice parameter values reported by Gerlach et al. for ion-assisted deposition (IAD)-grown GdN thin films capped by GaN as a protective layer[9] as well as to the values we obtained before.[11] It is reported that the lattice parameter value of GdN is dependent on the amount of impurities (oxygen) incorporated in the RE nitride material. For a material with the composition $Gd_{1.00}N_{0.88}O_{0.12}$, the lattice parameter changes to 4.96 ± 0.01 Å. When comparing this value to the values obtained here, it can be assumed that the amount of oxygen incorporated into the GdN thin films is quite low.

Nuclear reaction analysis (NRA) and Rutherford backscattering analysis (RBS) were performed to quantify the atomic ratio of the light elements C/N and O/N (NRA) and the ratio between the light elements and Gd, that is, Gd/N, Gd/C, and Gd/O (RBS), throughout the film. The data obtained for films deposited in the presence of ammonia are compiled in Table 6 (all RBS plots; see Figure 10). In addition to the signals of Gd and O, the RBS spectra show the presence of Cu, which arises from the capping layer. It should be noted that the analysis of the film deposited at 750 °C is difficult because the Cu layer on the top of the GdN layer is nonuniform. There is an overlap of the Cu and Gd peaks in the RBS spectrum (due to the increased film thickness of GdN), which makes it difficult to determine accurate values for the metal-to-nitrogen/carbon/oxygen ratios. We have a three-layer system consisting of a Cu layer on top, followed by a GdN film with high oxygen content at the interface between Cu and GdN, and, below, an almost pure GdN thin film. This is a hint for a Cu layer that was not efficient as a protective layer in this case. This is also observed in NRA, showing an O/N ratio of 0.98 ± 0.10. The carbon content in the film shows a C/N ratio of 0.01 ± 0.22 as an upper limit. The shape of the signals obtained by RBS show a decreasing oxygen concentration throughout the film, also supporting an oxygen diffusion through the Cu capping into the GdN thin film. However, as mentioned before, these values have to be used with care. Compared to this, the film deposited at 450 °C can be analyzed more accurately. A low O/N value of 0.02 ± 0.07 was found in NRA. This can possibly be explained by oxygen diffusion along grain boundaries of the Cu layer when the films are handled in air for some time, as it was in

dx.doi.org/10.1021/ic301826s | Inorg. Chem. 2013, 52, 286−296

Table 5. Calculated Lattice Parameters for GdN Deposited on Si(100)

deposition temp [°C]	2θ position [deg]	fwhm [deg]	lattice parameter [Å]
750	36.137	0.216	4.971 ± 0.005
850	36.095	0.241	4.977 ± 0.005

Table 6. Ratios of the Elements inside the GdN Films Deposited with Ammonia as Reactive Gas Obtained from RBS and NRA Analysis

deposition temp [°C]	RBS M/N	RBS M/C	RBS M/O	NRA C/N	NRA O/N
750	0.80	[a]	[a]	0.01 ± 0.22	0.98 ± 0.10
450	0.52	1.87	21.67	0.28 ± 0.18	0.02 ± 0.07

[a]Exact determination of the values was very difficult due to a nonuniformity of the Cu layer, as described above.

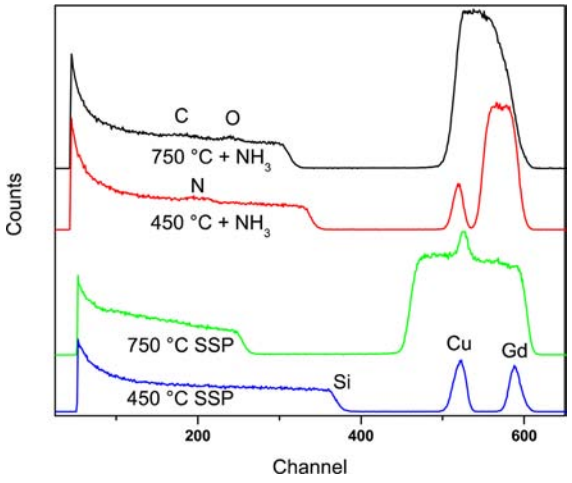

Figure 10. RBS spectra of films deposited using precursor **5** with ammonia (black and red) and under SSP conditions (green and blue).

the case when the films were prepared for the NRA and RBS measurements. Nevertheless, the Cu layer slows down the oxidation process of the GdN film and prevents complete oxidation. Also, the C/N ratio obtained from NRA measurements shows a quite low value of about 0.3. This value is in good agreement with the data reported before.[11] RBS measurements reveal that we have nitrogen-rich thin films with a Gd/N ratio of 0.52, showing that ammonia causes a sufficient N-incorporation into the films. The films deposited under SSP conditions have C/N values of 1.5 up to 7.1, showing a high C-incorporation into the films in the absence of ammonia.

EXPERIMENTAL SECTION

General Procedures. All reactions and manipulations are performed using standard Schlenk techniques under an atmosphere of argon. Sample preparation for analysis is carried out in an argon-filled glovebox. The solvents (technical grade) THF and pentane are dried and purified by an MBraun solvent purification system and stored over molecular sieves (4 Å). The starting compounds $GdCl_3$ (ABCR), *N,N′*-diisopropylcarbodiimide (Acros), MeLi, EtLi, ^{n}BuLi, and ^{t}BuLi (all from Fluka) and *N*-ethyl-*N′*-*tert*-butyl-carbodiimide (Sigma-Aldrich) are used as received. The lithium *N,N′*-diisopropyl-2-alkyl-amidinato ligands [Li{(N^iPr)$_2$CR}] are synthesized following modified literature procedures.[38,39]

Elemental analyses were performed by the analytical service of the Chemistry Department at the Ruhr-University Bochum (CHNSO Vario EL 1998). Electronic ionization (EI) mass spectra were recorded using a JEOL AccuTOF GCv. For high-resolution mass spectrometry (HR-MS), perfluorokerosine was used as a reference substance to determine the exact masses of the peaks. The thermal analysis data were obtained on a Seiko TGA/DTA 6300S11 instrument, which is operated outside a glovebox under ambient conditions. The measurements were carried out in aluminum crucibles with approximately 10 mg of sample under a nitrogen flow (99.9999%) of 300 mL/min, and a heating rate of 5 °C was employed. FT-IR spectroscopy was performed on a Bruker Alpha (ATR) spectrometer. The samples were prepared and measured inside a glovebox (MBraun, O_2 and H_2O content below 1 ppm). The intensities are abbreviated as follows: s, strong; m, medium; w, weak.

Synthesis and Characterization. *Gadolinium Tris(N,N′-diisopropyl-2-methyl-amidinate) [Gd{(N^iPr)$_2$CMe}$_3$] (**1**).* A solution of *N,N′*-diisopropylcarbodiimide (2.65 mL, 0.0173 mol) in 80 mL of THF is cooled to 0 °C, and to this an about 1.6 M solution of methyllithium in ether (10.5 mL, 0.0173 mol) is added dropwise. This mixture is allowed to warm to room temperature and stirred for 18 h under an inert atmosphere. The resulting pale yellow solution of [Li{(N^iPr)$_2$CMe}] is cooled to 0 °C and slowly added to a suspension of $GdCl_3$ (1.5 g, 0.0057 mol) in THF (60 mL). After warming to room temperature, the reaction mixture is stirred for 36 h under argon. The solvent is removed under reduced pressure, and the product is extracted in pentane, which is then filtered through a Celite pad to afford a pale yellow solution. A saturated solution is formed by removing part of the pentane under vacuum, and this solution is cooled to −20 °C to afford colorless crystals. However, they were not suitable for single-crystal X-ray analysis. A pure colorless crystalline compound is obtained through sublimation at 125 °C (6×10^{-2} mbar). Yield: 1.8 g (58%)

EI-MS (70 eV) *m/z*, rel. int. [%]: 581 [21%], 566 [8%], 538 [17%], 440 [100%], 424 [13%], 396 [5%], 355 [7%], 314 [11%], 298 [5%], 275 [3%], 142 [15%], 84 [6%], 58 [16%], 42 [32%]. Elemental analysis Calcd [%]: C, 49.62; N, 14.47; H, 8.85. Found [%]: C, 48.98; N, 14.54; H, 9.23. IR [cm^{-1}]: 3633 (w), 2935 (s), 2897 (m), 2837 (m), 2575 (w), 1638 (w), 1472 (s), 1401 (s), 1363 (s), 1322 (s), 1191 (s), 1161 (s), 1112 (s), 1008 (m), 917 (w), 791 (s), 613 (m), 540 (m), 422 (m).

Compounds **2**−**5** are obtained employing the same synthetic procedure as in the case of [Gd{(N^iPr)$_2$CMe}$_3$] **1**, unless described otherwise.

*Gadolinium Tris(N,N′-diisopropyl-2-ethyl-amidinate) [Gd{(N^iPr)$_2$CEt}$_3$] (**2**).* Following the same procedure described for **1**, $GdCl_3$ (1 g, 0.0038 mol) is reacted with [Li{(N^iPr)$_2$CEt}] (0.0116 mol) in THF at 0 °C. After 36 h of stirring at room temperature under an inert atmosphere and the workup described above, the product is obtained as a colorless crystalline solid. The crystals obtained were not suitable for X-ray diffraction analysis. Sublimation temperature: 130 °C (6×10^{-2} mbar). Yield: 0.81 g (38%)

EI-MS (70 eV) *m/z*, rel. int. [%]: 623 [9%], 580 [17%], 486 [70%], 452 [12%], 452 [9%], 383 [8%], 328 [12%], 241 [4%], 98 [18%], 56 [100%], 43 [24%]. Elemental analysis Calcd [%]: C, 51.21; N, 13.49; H, 9.22. Found [%]: C, 51.05; N, 13.56; H, 9.01. IR [cm^{-1}]: 3633 (w), 2935 (s), 2897 (m), 2840 (m), 2580 (w), 1536 (m), 1457 (s), 1363 (s), 1324 (s), 1226 (m), 1186 (s), 1112 (m), 1057 (m), 1031 (m), 966 (m), 816 (w), 769 (m), 688 (w), 601 (m), 533 (m), 426 (m).

*Gadolinium Tris(N,N′-diisopropyl-2-tert-butyl-amidinate) [Gd{(N^iPr)$_2$C^{t}Bu}$_3$] (**3**).* The reaction of $GdCl_3$ (1.5 g, 0.0057 mol) with [Li{(N^iPr)$_2$C^{t}Bu}] (0.0173 mol) affords a colorless crystalline product after workup as described for **1**. Single crystals suitable for

dx.doi.org/10.1021/ic301826s | Inorg. Chem. 2013, 52, 286−296

X-ray diffraction were obtained from the recrystallization of **3** in pentane. Sublimation temperature: 135 °C (6×10^{-2} mbar). Yield: 2.62 g (65%)

EI-MS (70 eV) *m*/*z*, rel. int. [%]: 707 [2%], 524 [100%], 508 [8%], 480 [6%], 439 [9%], 356 [12%], 298 [7%], 183 [8%], 126 [11%], 84 [88%], 57 [45%], 43 [15%]. Elemental analysis Calcd [%]: C, 56.05; N, 11.88; H, 9.83. Found [%]: C, 55.34; N, 11.52; H, 10.26. IR [cm^{-1}]: 2941 (s), 2900 (m), 2841 (m), 1393 (s), 1363 (s), 1292 (s), 1159 (s), 1114 (m), 1006 (s), 920 (w), 866 (w), 802 (w), 714 (m), 653 (m), 546 (w), 448 (m).

*Gadolinium Tris(N,N′-diisopropyl-2-n-butyl-amidinate) [Gd{(N^iPr)$_2C^nBu$}$_3$] (**4**).* Following the same procedure described for **1**, $GdCl_3$ (1 g, 0.0038 mol) is reacted with [Li{(N^iPr)$_2C^nBu$}] (0.0114 mol) in THF at 0 °C and stirred for 36 h at room temperature. After a workup described above, the product is obtained as a yellow viscous compound. Yield: 1.41 g (52%)

EI-MS (70 eV) *m*/*z*, rel. int. [%]: 707 [9%], 693 [9%], 666 [23%], 551 [16%], 524 [100%], 510 [19%], 478 [15%], 440 [12%], 395 [9%], 357 [15%], 143 [24%], 113 [20%], 83 [100%], 57 [42%], 42 [29%]. Elemental analysis Calcd [%]: C, 56.05; N, 11.88; H, 9.83. Found [%]: C, 56.27; N, 11.03; H, 9.14. IR [cm^{-1}]: 3415 (w), 2935 (s), 2897 (m), 2841 (m), 1605 (m), 1461 (s), 1410 (m), 1364 (m), 1327 (m), 1186 (s), 1114 (m), 1040 (m), 970 (w), 880 (w), 821 (m), 775 (w), 674 (w), 603 (m), 429 (m).

*Gadolinium Tris(N-tert-butyl-N′-ethyl-2-methyl-amidinate) [Gd{(NEt)(N^tBu)CMe}$_3$] (**5**).* The reaction of $GdCl_3$ (2 g, 0.0076 mol) with [Li{(NEt)(N^tBu)CMe}] (0.0228 mol) in THF at 0 °C affords a white to pale gray crystalline product. After workup as described for **1**, a colorless crystalline solid is obtained. Crystals grown from pentane were suitable for single crystal X-ray analysis. Sublimation temperature: 120 °C (6×10^{-2} mbar). Yield: 3.1 g (68%)

EI-MS (70 eV) *m*/*z*, rel. int. [%]: 581 [3%], 566 [4%], 524 [59%], 440 [100%], 424 [40%], 408 [34%],382 [22%], 354 [6%], 314 [6%], 298 [20%], 240 [14%], 127 [2%], 84 [17%], 58 [48%], 42 [37%]; Elemental analysis Calcd [%]: C, 49.62; N, 14.47; H, 8.85. Found [%]: C, 48.47; N, 14.72; H, 8.58. IR [cm^{-1}]: 2935 (s), 2840 (m), 2638 (w), 1474 (s), 1393 (s), 1324 (s), 1202 (s), 1144 (s), 1080 (m), 1023 (m), 970 (m), 806 (m), 755 (m), 631 (m), 564 (m), 532 (m), 473 (m), 439 (w).

X-ray Structure Determination. The X-ray intensity data for **3**·0.5 C_5H_{12} were measured in the ω scan mode on an Oxford Diffraction Xcalibur2 diffractometer, using graphite monochromated Mo Kα radiation. CrysAlis^{Pro} (CrysAlis^{Pro}, version 1.171.35.19, Agilent Technologies, Yarnton, Oxfordshire, U.K.) was used to operate the diffractometer and to process the data. A semiempirical absorption correction based on multiple-scanned reflections was applied.[44] The intensity data of **5** were collected on a Stoe IPDS 2T diffractometer with Mo Kα radiation. The data were collected with the Stoe XAREA program using ω-scans (XRED32 included in XAREA, Stoe, 2002). The crystal structures were solved by direct methods using SHELXS-97 and refined by full-matrix least-squares refinement on F^2 with SHELXL-97.[45] Anisotropic displacement parameters were introduced for all non-hydrogen atoms. Hydrogen atoms were placed at geometrically calculated positions and refined using a riding model. The crystal of **3**·0.5 C_5H_{12} was a nonmerohedral twin. The twin operation is a 2-fold rotation about the [100] direction. The final structure refinement was carried out using the HKLF 5 option of SHELXL-97, which resulted in a ratio of the twin components of 0.5108(5):0.4892(5). A *tert*-butyl group in **3**·0.5 C_5H_{12} shows rotational disorder over two positions, which was described by the split model. Refinement of the occupancies by means of a free variable yielded a ratio of 0.659(6):0.341(6). Standard similar distance restraints and equivalent anisotropic displacement parameters were used to model the disorder. Crystal data and refinement details are given in Table 1. The CCDC numbers of the compounds **3** and **5** are 895562 and 895439, respectively.

Thin-Film Deposition. MOCVD experiments were performed using **5** as the precursor, and thin films were grown on ultrasonically cleaned 2 in. p-type Si(100) substrates (SI-MAT). A home-built, horizontal low-pressure cold-wall reactor was employed for MOCVD experiments. Nitrogen (flow rate: 50 sccm, 99.9999%) and, if required, ammonia (flow rate: 50 sccm, 99.999%) were used as carrier or reactive gas, respectively. For each deposition, approximately 50 mg of the precursor was filled into a glass bubbler inside a glovebox. Depositions were carried out in the substrate temperature range of 350−850 °C, while the precursor vaporizer was maintained at 120 °C. Depositions were carried out for 10 min, and the reactor pressure was maintained at 1 mbar. In a subsequent step, a copper layer was deposited on top of the GdN thin film to avoid or slow down the oxidation of the as-deposited films. [Cu(dmap)$_2$] (dmap = 3-dimethylamino-propanolato) was used as the Cu source, and 50 mg of the precursor was filled in a second chamber of the bubbler.[46] The depositions were carried out at 300 °C while the precursor was kept at room temperature. The depositions were also carried out for 10 min at a reduced pressure of 0.1 mbar. This kind of protective layer was chosen for two reasons. The Cu-MOCVD using [Cu(dmap)$_2$] as precursor nicely matches the experimental conditions of the GdN MOCVD reactor setup and thus facilitates the direct capping of the deposited GdN layer in the same MOCVD screening reactor and avoiding any sample transfer. In addition, we deliberately avoided GaN capping (or similar oxidation-resistant metal nitride cappings) and chose a N-free capping material, which also matches well with the RBS and NRA analytical techniques in order to investigate the incorporation of N (and O, C) into the deposited film.

Film Characterization. The crystallinity of the films was investigated by X-ray diffraction (XRD) analysis using a Bruker D8 Advance AXS diffractometer [Cu Kα radiation (1.5418 Å)] with a position-sensitive detector (PSD). All films were analyzed in the $\theta-2\theta$ geometry. The surface morphology and the thickness of the films were analyzed by scanning electron microscopy (SEM) using a LEO Gemini SEM 1530 electron microscope. A combination of RBS and NRA (or: deuteron induced γ-ray emission, details see lit. 11) was performed to estimate the stoichiometry of the films and to quantify the atomic ratio of the light elements C/N and O/N (NRA) and the ratio between the light elements and Gd throughout the bulk of the film.

CONCLUSIONS

The synthesis, characterization, evaluation, and application of five different homoleptic gadolinium amidinate precursors are presented. Single-crystal X-ray diffraction data of **3** and **5** as representative examples of the series confirm the anticipated mononuclear homoleptic structure, in which Gd^{3+} is coordinated by three chelating amidinato ligands. Mass spectrometric analyses reveal that all compounds have a similar fragmentation behavior, but with some interesting differences related to possible β-H elimination depending on the alkyl group substitution pattern at the amidinate ligands. Interestingly, the alkyl-substitution pattern offers some control over the physical (onset of volatilization) and chemical properties (onset of decomposition) of the compounds. The asymmetrically substituted compound **5** exhibits the best thermal properties, and it was used for preliminary MOCVD experiments to deposit GdN thin films under single source (SSP) conditions and as well as with ammonia as reactive gas and an additional N source. Rock-salt structured and essentially C- and O-free GdN thin films are obtained only in the latter case. The protective capping of the as-deposited GdN thin film materials for preventing postdeposition oxidation remains a problem that needs further work in order to proceed to a more detailed and significant materials characterization (e.g., magnetic measurements). Nevertheless, our data on the homologous series of alkyl-substituted, homoleptic tris-amidinates of gadolinium hold promise for a further development of this kind of compound as precursors for RE nitride materials.

dx.doi.org/10.1021/ic301826s | *Inorg. Chem.* 2013, 52, 286−296

■ ASSOCIATED CONTENT

Supporting Information

EI-MS data of compounds **3** and **4**, growth rates of the thin films deposited using precursor **5**, and crystallographic data are available. This material is available free of charge via the Internet at http://pubs.acs.org.

■ AUTHOR INFORMATION

Corresponding Author

*E-mail: anjana.devi@rub.de (A.D.), frank.edelmann@ovgu.de (F.T.E.).

Notes

The authors declare no competing financial interest.

■ ACKNOWLEDGMENTS

The authors thank the Ruhr-University Bochum Research School for financial support. Dr. T. B. Thiede is acknowledged for helpful discussions and for critical comments on the manuscript. Dr. R. Neuser and Mr. M. Born are acknowledged for their SEM measurements. In addition, the authors want to thank the Ruhr-University Bochum Materials Research Department (MRD).

■ REFERENCES

(1) Aerts, C.; Strange, P.; Horne, M.; Temmerman, W.; Szotek, Z.; Svane, A. *Phys. Rev. B* **2004**, *69*, 045115.
(2) Khazen, K.; von Bardeleben, H.; Cantin, J.; Bittar, A.; Granville, S.; Trodahl, H.; Ruck, B. *Phys. Rev. B* **2006**, *74*, 245330.
(3) Granville, S.; Ruck, B.; Budde, F.; Koo, A.; Pringle, D.; Kuchler, F.; Preston, A.; Housden, D.; Lund, N.; Bittar, A.; Williams, G.; Trodahl, H. *Phys. Rev. B* **2006**, *73*, 235335.
(4) Leuenberger, F.; Parge, A.; Felsch, W.; Fauth, K.; Hessler, M. *Phys. Rev. B* **2005**, *72*, 014427.
(5) Zhou, Y. K.; Kim, M. S.; Teraguchi, N.; Suzuki, A.; Nanishi, Y.; Asahi, H. *Phys. Status Solidi B* **2003**, *240*, 440.
(6) Ludbrook, B. M.; Farrell, I. L.; Kuebel, M.; Ruck, B. J.; Preston, A. R. H.; Trodahl, H. J.; Ranno, L.; Reeves, R. J.; Durbin, S. M. *J. Appl. Phys.* **2009**, *106*, 063910.
(7) Vidyasagar, R.; Kitayama, S.; Yoshitomi, H.; Kita, T.; Sakurai, T.; Ohta, H. *Appl. Phys. Lett.* **2012**, *100*, 232410.
(8) Scarpulla, M. A.; Gallinat, C. S.; Mack, S.; Speck, J. S.; Gossard, A. C. *J. Cryst. Growth* **2009**, *311*, 1239.
(9) Gerlach, J. W.; Mennig, J.; Rauschenbach, B. *Appl. Phys. Lett.* **2007**, *90*, 061919.
(10) McKenzie, W. R.; Munroe, P. R.; Budde, F.; Ruck, B. J.; Granville, S.; Trodahl, H. J. *Curr. Appl. Phys.* **2006**, *6*, 407.
(11) Thiede, T. B.; Krasnopolski, M.; Milanov, A. P.; de los Arcos, T.; Ney, A.; Becker, H.-W.; Rogalla, D.; Winter, J.; Devi, A.; Fischer, R. A. *Chem. Mater.* **2011**, *23*, 1430.
(12) Milanov, A. P.; Thiede, T. B.; Devi, A.; Fischer, R. A. *J. Am. Chem. Soc.* **2009**, *131*, 17062.
(13) Brewer, J. R.; Gernhart, Z.; Liu, H.; Cheung, C. L. *Chem. Vap. Deposition* **2010**, *16*, 216.
(14) Edelmann, F. T. *Chem. Soc. Rev.* **2009**, *38*, 2253.
(15) Kukli, K.; Ritala, M.; Pore, V.; Leskela, M.; Sajavaara, T.; Hegde, R. I.; Gilmer, D. C.; Tobin, P. J.; Jones, A. C.; Aspinall, H. C. *Chem. Vap. Deposition* **2006**, *12*, 158.
(16) Triyoso, D.; Hegde, R. I.; Grant, J. M.; Schaeffer, J. K.; Roan, D.; White, B. E.; Tobin, P. J. *J. Vac. Sci. Technol., B* **2005**, *23*, 288.
(17) Kukli, K.; Ritala, M.; Pilvi, T.; Sajavaara, T.; Leskelä, M.; Jones, A. C.; Aspinall, H. C.; Gilmer, D. C.; Tobin, P. J. *Chem. Mater.* **2004**, *16*, 5162.
(18) Jones, A. C.; Aspinall, H. C.; Chalker, P. R.; Potter, R. J.; Kukli, K.; Rahtu, A.; Ritala, M.; Leskela, M. *J. Mater. Chem.* **2004**, *14*, 3101.
(19) He, W.; Schuetz, S.; Solanki, R.; Belot, J.; McAndrew, J. *Electrochem. Solid-State Lett.* **2004**, *7*, G131.
(20) Gordon, R. G.; Becker, J.; Hausmann, D.; Suh, S. *Chem. Mater.* **2001**, *13*, 2463.
(21) Fitzmaurice, J.; Hector, A.; Rowley, A.; Parkin, I. *Polyhedron* **1994**, *13*, 235.
(22) LaDuca, R.; Wolczanski, P. *Inorg. Chem.* **1992**, *31*, 1311.
(23) Gun'ko, Y. K.; Edelmann, F. T. *Comments Inorg. Chem.* **1997**, *19*, 153.
(24) Päiväsaari, J.; Niinistö, J.; Arstila, K.; Kukli, K.; Putkonen, M.; Niinistö, L. *Chem. Vap. Deposition* **2005**, *11*, 415.
(25) Niinistö, J.; Petrova, N.; Putkonen, M.; Niinistö, L.; Arstila, K.; Sajavaara, T. *J. Cryst. Growth* **2005**, *285*, 191.
(26) Scarel, G.; Bonera, E.; Wiemer, C.; Tallarida, G.; Spiga, S.; Fanciulli, M.; Fedushkin, I. L.; Schumann, H.; Lebedinskii, Y.; Zenkevich, A. *Appl. Phys. Lett.* **2004**, *85*, 630.
(27) Niinistö, J.; Putkonen, M.; Niinistö, L. *Chem. Mater.* **2004**, *16*, 2953.
(28) Putkonen, M.; Nieminen, M.; Niinistö, J.; Niinistö, L.; Sajavaara, T. *Chem. Mater.* **2001**, *13*, 4701.
(29) Whitney, P.; Uwai, K.; Nakagome, H.; Takahei, K. *Appl. Phys. Lett.* **1988**, *53*, 2074.
(30) Uwai, K.; Nakagome, H.; Takahei, K. *J. Cryst. Growth* **1988**, *93*, 583.
(31) Baisch, U.; Pagano, S.; Zeuner, M.; Barros, N.; Maron, L.; Schnick, W. *Chem.—Eur. J.* **2006**, *12*, 4785.
(32) de Rouffignac, P.; Park, J.; Gordon, R. *Chem. Mater.* **2005**, *17*, 4808.
(33) Lim, B. S.; Rahtu, A.; de Rouffignac, P.; Gordon, R. *Appl. Phys. Lett.* **2004**, *84*, 3957.
(34) Lim, B. S.; Rahtu, A.; Park, J.; Gordon, R. *Inorg. Chem.* **2003**, *42*, 7951.
(35) Lim, B. S.; Rahtu, A.; Gordon, R. *Nat. Mater.* **2003**, *2*, 749.
(36) Milanov, A. P.; Xu, K.; Laha, A.; Bugiel, E.; Ranjith, R.; Schwendt, D.; Osten, H. J.; Parala, H.; Fischer, R. A.; Devi, A. *J. Am. Chem. Soc.* **2010**, *132*, 36.
(37) Milanov, A. P.; Toader, T.; Parala, H.; Barreca, D.; Gasparotto, A.; Bock, C.; Becker, H. W.; Ngwashi, D. K.; Cross, R.; Paul, S.; Kunze, U.; Fischer, R. A.; Devi, A. *Chem. Mater.* **2009**, *21*, 5443.
(38) Dröse, P.; Blaurock, S.; Hrib, C. G.; Edelmann, F. T. *Z. Anorg. Allg. Chem.* **2010**, *637*, 186.
(39) Aeilts, S.; Coles, M.; Swenson, D.; Jordan, R.; Young, V. *Organometallics* **1998**, *17*, 3265.
(40) Milanov, A. P.; Fischer, R. A.; Devi, A. *Inorg. Chem.* **2008**, *47*, 11405.
(41) Rowley, C. N.; DiLabio, G. A.; Barry, S. T. *Inorg. Chem.* **2005**, *44*, 1983.
(42) Scherrer, P. *Nachr. Ges. Wiss. Goettingen, Math.-Phys. K1., Fachgruppe 1* **1918**, 98.
(43) Gambino, R. J.; Cuomo, J. J. *J. Electrochem. Soc.* **1966**, *113*, 401.
(44) Blessing, R. H. *Acta Crystallogr.* **1995**, *A51*, 33.
(45) Sheldrick, G. M. *Acta Crystallogr.* **2008**, *A64*, 112.
(46) Becker, R.; Devi, A.; Weiss, J.; Weckenmann, U.; Winter, M.; Kiener, C.; Becker, H. W.; Fischer, R. A. *Chem. Vap. Deposition* **2003**, *9*, 149.